DOI: 10.1002/ejic.200801244

The Nature of the Metal–Carbene Bond in Normal and Abnormal Pyridylidene, Quinolylidene and Isoquinolylidene Complexes[‡]

Greta Heydenrych,[a] Moritz von Hopffgarten,[a] Elzet Stander,[b] Oliver Schuster,[b] Helgard G. Raubenheimer,*[b] and Gernot Frenking*[a]

Keywords: Density functional calculations / Carbenes / Carbene homologs / Carbene ligands / Nitrogen heterocycles / Pyridylidene / Quinolylidene / Pyridyl complexes / Metal–carbon bonds / Energy-decomposition analysis

Quantum chemical calculations using DFT at the BP86/TZ2P level of theory are reported for the complexes $(PH_3)_2ClM$-L where L is an N-heterocyclic ligand and M a group-10 metal Ni, Pd and Pt. The ligands comprise pyridyl groups or carbenes derived from the pyridine, quinolidine or isoquinolidine systems wherein the nitrogen atom is either adjacent to the carbene carbon atom or it is in a remote (*meta* or *para*, or in the adjacent ring) position. Comparative calculations include the isomeric ligands of the well-known five-membered N-heterocyclic carbene. The nature of the metal–ligand interactions are investigated by energy decomposition analysis (EDA). The EDA results suggest that the nature of the metal–carbene bonds in the complexes shows little variation when the position of the nitrogen atom in pyridylidenes is adjacent (*ortho*) or remote (*meta* or *para*). It changes even very little when the nitrogen atom is in an adjacent ring to the cyclic carbene moiety. The most significant differences between the bond strengths come from the energy level of the σ-HOMO of the carbene ligand which depends largely on the position of the nitrogen atom. An energetically higher-lying σ lone-pair orbital of the carbene ligand yields stronger orbital interactions but also stronger electrostatic attraction because of better overlap with the metal nucleus. This holds also for the isomers of the five-membered N-heterocyclic carbenes. An excellent correlation is established between the ε(HOMO) values of the ligands and the metal–ligand interaction energies, ΔE_{int}.

Introduction

Since Arduengo's report on a stable 2-imidazolylidene (Figure 1, **A**) almost two decades ago,[1] reports on N-heterocyclic carbenes (NHCs) largely focussed on ligands with a similar design, i.e. five-membered cycles with two stabilising nitrogen atoms adjacent to the carbene carbon.[2] As a consequence, the term NHC tends to be misused as a synonym for this kind of ligands. However, Crabtree's finding of an "*abnormally*" bound 4-imidazolylidene (**B**) sensitised the scientific community not only to the variable nature of NHCs but also to the fact, that less stabilised carbenes could exhibit certain desired properties. Accordingly, the interest in "non-classical" N-heterocyclic carbenes is growing rapidly.[3]

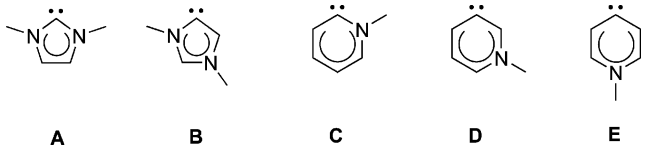

Figure 1. Idealised singlet representation of N-heterocyclic carbenes with empty p_π-carbene orbitals.

During the last decade, we have been particularly interested in pyridylidenes (**C**, **D**, **E**; Figure 1) owing to their ability to form *normal*, *abnormal* and *remote* carbenes.[4–8] Generally we consider a carbene to be *abnormal* if no formal neutral carbene Lewis structure can be drawn and to be *remote* if there is no heteroatom adjacent to the carbene carbon.[3] Note that in this sense, **D** is *abnormal* and *remote* (Figure 2) while **E** is *normal* and *remote*. As an extension of the concept we have also synthesised and fully characterised quinolinium and isoquinolinium derived carbene complexes (selected examples shown in Figure 3) that include the carbene carbon within (**d**, **e**)[5,6,9,10] or outside (**f**, **g**)[11] the N-containing ring. The latter arrangement provides the possibility of extending the remoteness to five bonds (**g**).

The nature of the metal–carbene bond in *normal* 2-imidazolylidene complexes has been investigated in a large number of theoretical studies.[12] Recently, some of us have

[‡] Theoretical Studies of Organometallic Compounds, 62. Part 61: S. Erhardt, G. Frenking, *J. Organomet. Chem.*, in print.

[a] Fachbereich Chemie, Philipps-Universität Marburg, Hans-Meerwein-Strasse, 35043 Marburg, Germany
Fax: +49-6424-282-5566
E-mail: frenking@chemie.uni-marburg.de
[b] Department of Chemistry and Polymer Science, University of Stellenbosch, Private Bag X1, Matieland 7602, South Africa
E-mail: hgr@sun.ac.za

Supporting information for this article is available on the WWW under http://www.eurjic.org or from the author.

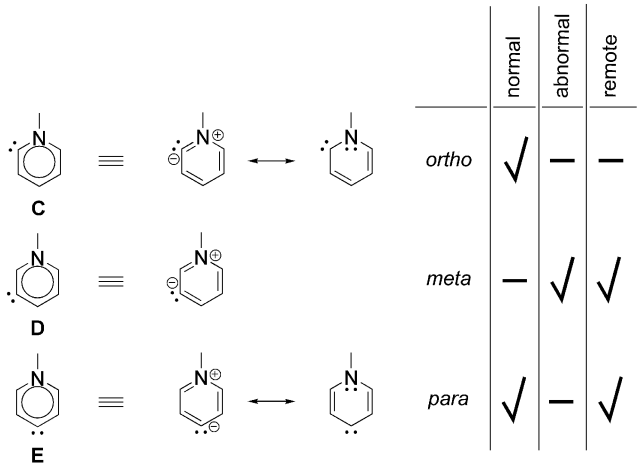

Figure 2. Representation and canonical structures of pyridinium-derived carbenes taking π-stabilisation of the formal empty p_π-carbene orbital into account.

likewise reported on the bonding properties of their *abnormal* 4-imidazolylidene congeners.[13] Electrostatic interactions dominate the bond formation whereas the orbital overlap consists mainly of a σ component. It is believed that metal–ligand π-back-donation makes a small contribution, because the N-atom(s) adjacent to the carbene carbon donate π-electron density into the formally empty p-orbital on the singlet carbene carbon, thus limiting the ligand's inclination to accept electron density from the metal atom.[14–16] This tendency is amplified upon coordination to a metal centre.[17,18] Aromaticity within the heterocycle also contributes to the N→C π-donation, so that upon coordination, unsaturated 2-imidazolylidenes are more stable than saturated 2-imidazolidinylidene counterparts.[19] Moreover, even though the difference in relative bond-dissociation energies between such saturated and unsaturated carbene complexes is rather small, their catalytic properties are quite different.[20] While it is already well-known that NHCs are more basic and stronger donors than phosphanes, it has also been claimed that substitution has a smaller effect on imidazolylidenes than on phosphanes.[13,21]

In first reports on pyridylidenes and their complexes, we have demonstrated that in accordance with the results for other carbenes, most of the attraction between the ligand and the metal centre is also electrostatic and that the covalent contribution again mostly constitutes σ-interaction.[5,10] Schwarz et al. have supported their detection of stable pyridylidenes under high vacuum conditions by calculations of the relative stabilities of *free* pyridylidene isomers compared to pyridine.[22] Herein we now describe our results when, for the first time, *ortho*-, *meta* and *para*-model pyridylidene complexes **4M**–**6M** – wherein the carbenes **4**–**6** (Figure 4) are complexed to $(PH_3)_2ClM$ (M = Ni, Pd, Pt) and occur *trans* to Cl – are compared with their pyridyl precursors **1M**–**3M** (with **1**–**3** acting as anionic ligands). We were particularly interested in how the metal–carbene bond is affected by remoteness of the one nitrogen atom and also by the *normality* or *abnormality* of the ligand. Moreover, we also investigated quinolylidene and isoquinolylidene model complexes wherein the carbene carbon of the ligands (**7**–**22**) is located in the carbocyclic ring. In order to compare our new results to a class of N-heterocyclic ligands that is already theoretically better understood, the model *normal* and *abnormal* imidazolylidene complexes of ligands **23** and **24** were also included in the study.

Computational Methods

All geometries were optimized under C_s-symmetry constraint with density-functional theory at the BP86 level of theory[23] using uncontracted Slater-type orbitals (STOs) with TZ2P quality as basis functions for the SCF calculations.[24] An auxiliary set of s, p, d, f, and g STOs was used to fit the molecular densities and to represent the Coulomb and exchange potentials accurately in each SCF cycle.[25] Scalar relativistic effects have been incorporated by applying the zeroth-order regular approximation (ZORA).[26] The nature of the stationary points on the potential-energy surface was determined by calculating the vibrational frequencies. All structures are minima on the potential-energy surface (PES) unless otherwise noted.

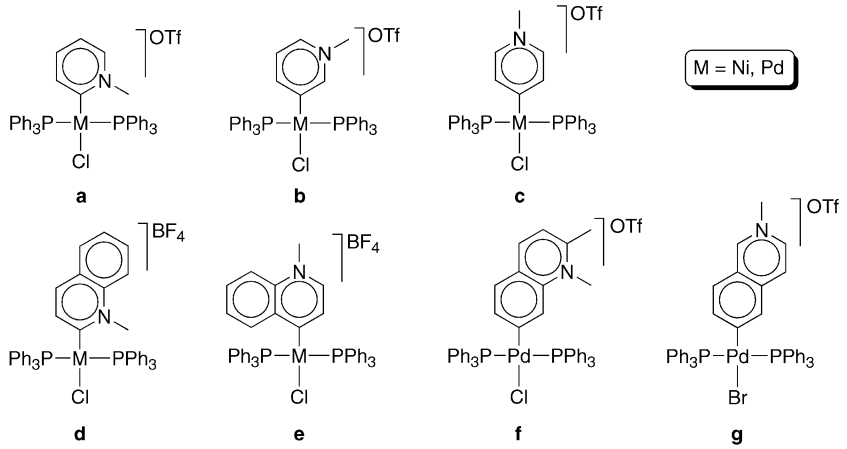

Figure 3. Examples of known pyridinium-derived N-heterocyclic carbene complexes.[7]

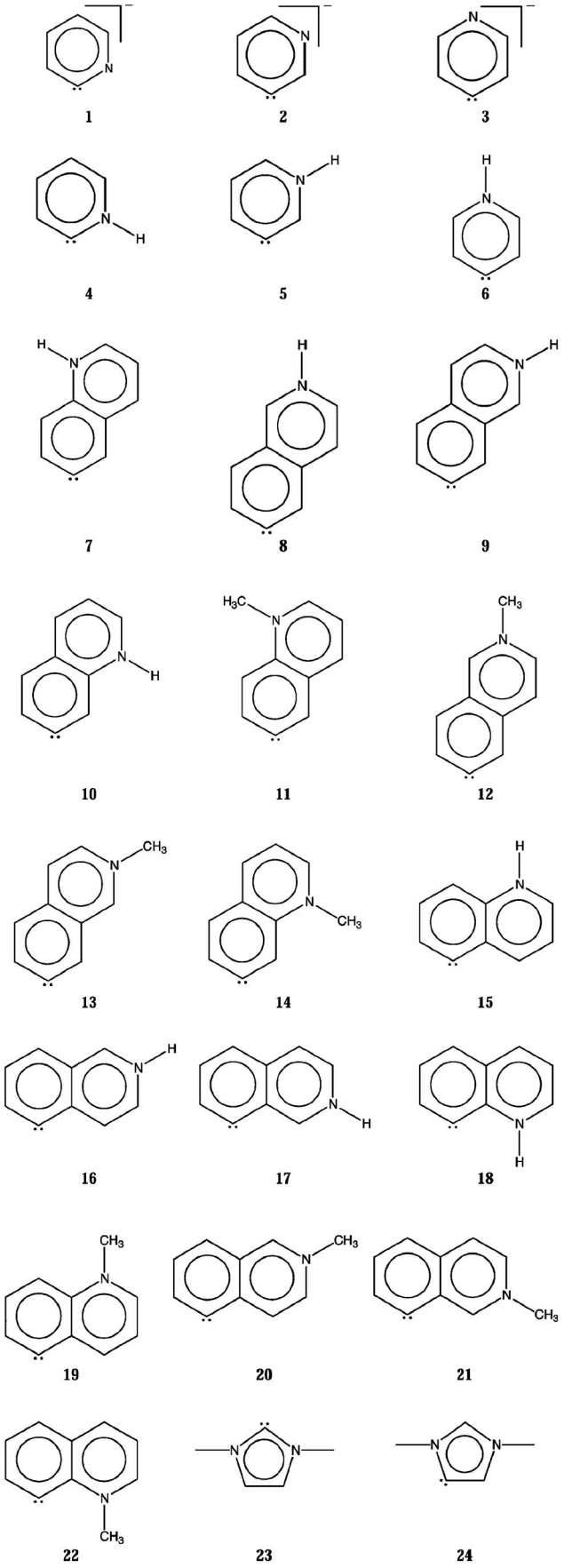

Figure 4. N-Heterocyclic ligands investigated in this work.

The bonding situation of the metal–carbene bonds was investigated by an energy-decomposition analysis (EDA) which was developed by Morokuma[27] and by Ziegler and Rauk.[28] The bonding analysis focuses on the instantaneous interaction energy ΔE_{int} of a bond A–B between two fragments A and B in the particular electronic reference state and in the frozen geometry of AB. This interaction energy is divided into three main components [Equation (1)].

$$\Delta E_{int} = \Delta E_{elstat} + \Delta E_{Pauli} + \Delta E_{orb} \quad (1)$$

The term ΔE_{elstat} corresponds to the classical electrostatic interaction between the unperturbed charge distributions of the prepared atoms and is usually attractive. The Pauli repulsion ΔE_{Pauli} is the energy change associated with the transformation from the superposition of the unperturbed electron densities $\rho_A + \rho_B$ of the isolated fragments to the wavefunction $\psi^0 = N\hat{A}[\psi_A\psi_B]$, which properly obeys the Pauli principle through explicit antisymmetrization ($\hat{A}$ operator) and renormalization of the product wavefunction.[29] It comprises the destabilizing interactions between electrons of the same spin on either fragment. The orbital interaction ΔE_{orb} accounts for charge-transfer and polarization effects.[30] The ΔE_{orb} term can be decomposed into contributions from each irreducible representation of the point group of the interacting system. This makes it possible to estimate the intrinsic strength of orbital interactions from orbitals having a′ (σ) and a′′ (π) symmetry quantitatively. To obtain the bond-dissociation energy (BDE) D_e the preparation energy ΔE_{prep} which gives the relaxation of the fragments into their electronic and geometrical ground states must be added to ΔE_{int} [Equation (2)].

$$\Delta E(= -D_e) = \Delta E_{int} + \Delta E_{prep} \quad (2)$$

To calculate the dissociation energies, we calculated each fragment in its optimized geometry and derived ΔE by Equation (2). Further details on the EDA can be found in the literature.[29,31] The EDA has been used by us for a comprehensive study of metal–ligand interactions in transition metal complexes.[32]

Geometries and Energies

Figure 5 gives the most important bond lengths which have been calculated for the equilibrium geometries of the pyridyl complexes **1M**–**3M** and the carbene compounds **4M**–**6M** at BP86/TZ2P. The geometries were optimized with C_s symmetry constraints where the dihedral angle H_3P–M–C–N was either fixed at 90° (perpendicular form) or at 0° (planar form). It turned out that the perpendicular structures which are shown in Figure 5 are minima on the PES while the energetically higher lying planar forms are transition states for rotation about the M–C bond. A notable exception is the platinum complex **1Pt** where the planar form is 1.36 kcal/mol lower in energy than the perpendicular structure which is a transition state. Table 1 gives

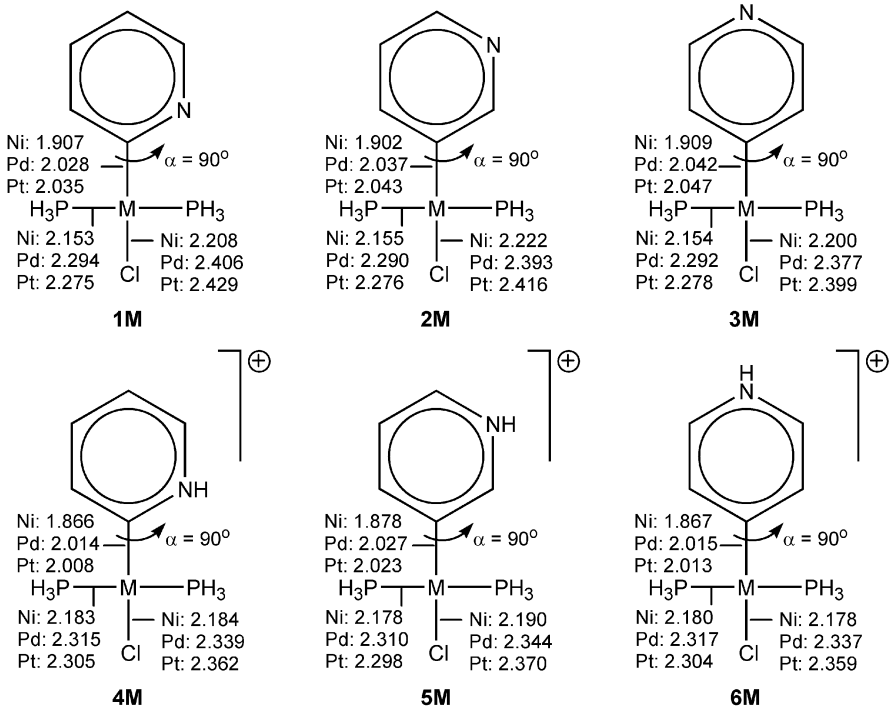

Figure 5. Schematic representation of the calculated pyridyl complexes **1M**–**3M** and pyridylidene complexes **4M**–**6M**, respectively (M = Ni, Pd, Pt). The optimised M–C, M–PH_3 and M–Cl bond lengths are given in Å. The perpendicular arrangement of the ligands and the $M(PH_3)_2Cl$ fragment is indicated by α.

the relative energies of the perpendicular and planar forms of **1M**–**6M**. The relative energies of the free ligands **1**–**6** are also given.

The calculated energies of both neutral and cationic classes of compounds **1M**–**6M** (Table 1) suggest that the *ortho* complexes are more stable than the *meta* and *para* forms. The relative energies of the *ortho*, *meta* and *para* isomers of the *N*-protonated carbene complexes **4M**–**6M** exhibit larger variations than the neutral complexes **1M**–**3M** where the *ortho* form is only slightly lower in energy than the *meta* and *para* isomers. We point out that the stability order does not always correlate with the metal–carbon bond lengths of **1M**–**6M**. It has been noted before that metal–ligand bond lengths often do not correlate with the bond strength.[33] The calculated barriers for rotation about the metal–carbon bond of the *ortho* forms **1M** are very low; as noted before, the planar form of **1Pt** is even 1.36 kcal/mol lower in energy than the perpendicular form. The rotational barriers of **2M** and **3M** are somewhat higher. The cationic carbene complexes **4M**–**6M** also have higher rotational barriers supposedly owing to more metal–ligand π-bonding in these species. This assumption will be discussed below when we present the EDA results. Finally, it can be noted that rotation becomes more facile with increasing radius of the metal center.

A very interesting result given in Table 1 is the comparison of the relative energies of the free ligands **1**–**6** with the relative energies of the corresponding complexes **1M**–**6M**. The *ortho* form of the free pyridyl **1** is clearly higher in energy than the *meta* and *para* isomers **2** and **3** but the complexes **1M** are slightly more stable than **2M** and **3M**, respectively. This means that the metal–ligand interactions in **1M** are stronger than the bonding in **2M** and **3M** thus compensating for the energy difference between the free ligands. The relative energy difference between **2** and **3** hardly changes when the ligands become bonded in **2M** and **3M** which suggests that the metal–ligand bond strengths in the *meta* and *para* complexes are similar. Notably, the opposite trend in the relative energies of the ligands and in the alteration upon complexation is predicted for the carbenes **4**–**6**. First, the *ortho* form of the free carbene 4 is now significantly *lower* in energy than the *meta* isomer **5** and the *para* species **6**, respectively (Table 1). Second, the energy difference *decreases* for the complexes **4M**–**6M** which means that the metal–ligand interaction in the *ortho* form **4M** is *weaker* than in the respective *meta* and (particularly) the *para* isomers **5M** and **6M**. However, the stronger metal–ligand bonds in the latter species do not compensate for the energy difference between the ligands since the *ortho* form **4M** remains more stable than the *meta* and *para* isomers. The general conclusion is that the less stable free ligand yields stronger metal–ligand bonds.

Figure 6 shows the calculated equilibrium geometries of the quinolylidene and isoquinolylidene complexes **7M**–**22M** wherein the heteroatom appears in a neighbouring aromatic ring. Compounds **7M**–**10M** have *N*-protonated quinolylidene and isoquinolylidene ligands with the metal fragment bonded to the carbene carbon atom which occurs in the β position to the annelated benzene ring. Compounds **11M**–

Table 1. Relative energies [kcal/mol] of the calculated model complexes **1M**–**24M** and the free ligands L at the RI–BP86/TZ2P level. Energies of the HOMO of the free ligand ε(HOMO) [eV].

	Carbene structure		E_{rel}				ε(HOMO)
	Normal or abnormal	Adjacent or remote	M = Ni	M = Pd	M = Pt	L	L
Pyridyl							
1M			0.00	0.00	0.00	0.00	+1.852
2M			1.41	1.96	1.22	–8.44	+1.318
3M			0.74	1.72	0.70	–9.62	+1.283
1M(planar)			4.00	2.05	–1.36		–
2M(planar)			11.77	8.67	6.22		–
3M(planar)			11.64	8.61	5.93		–
Pyridylidene							
4M	normal	adjacent	0.00	0.00	0.00	0.00	–4.281
5M	abnormal	remote	5.50	5.31	6.17	13.76	–3.673
6M	normal	remote	5.53	5.48	5.34	16.50	–3.515
4M(planar)	normal	adjacent	12.76	9.18	8.10		–
5M(planar)	abnormal	remote	17.47	13.72	13.27		–
6M(planar)	normal	remote	15.35	11.93	10.27		–
N-Protonated (iso)quinolylidene							
7M	abnormal	remote	2.54	3.69	4.45	17.95	–2.932
8M	normal	remote	1.06	2.65	3.19	18.06	–2.941
9M	abnormal	remote	2.85	3.96	5.95	18.79	–2.894
10M	normal	remote	0.85	2.25	4.06	14.16	–3.092
15M	abnormal	remote	2.30	3.20	3.99	11.21	–3.129
16M	abnormal	remote	3.58	4.30	5.18	13.86	–3.126
17M	normal	remote	2.46	3.29	3.91	9.54	–3.322
18M	abnormal	remote	0.00	0.00	0.00	0.00	–3.732
N-Methylated (iso)quinolylidene							
11M	abnormal	remote	2.10	1.72	1.89	0.26	–2.826
12M	normal	remote	0.00	0.00	0.00	0.00	–2.837
13M	abnormal	remote	1.44	1.16	1.41	0.62	–2.784
14M	normal	remote	0.59	0.61	0.62	–3.22	–2.966
19M	normal	remote	1.90	1.35	1.51	–6.27	–3.012
20M	abnormal	remote	1.64	0.96	1.21	–4.57	–3.006
21M	normal	remote	1.37	0.68	0.75	–8.39	–3.211
22M	abnormal	remote	6.72	7.10	8.70	–16.26	–3.405
Imidazolylidene							
23M	normal	adjacent	0.00	0.00	0.00	0.00	–4.968
24M	abnormal	adjacent	6.98	6.89	7.30	17.37	–4.246

14M are the methylated analogues of the previous group. In complexes **15M**–**22M** the carbene carbon atom appears α to the annelated ring. We calculated only the orthogonal equilibrium geometries of the quinolylidene-type complexes. The relative energies of the protonated and methylated compounds are given in Table 1.

The energy values in Table 1 suggest that the position of the N–H and N–CH_3 moiety in the β-carbene complexes **7M**–**14M** generally have little influence on the relative stabilities of the isomers. There is also not much energy difference between the *N*-protonated β-carbene complexes **7M**–**10M** and the isomeric α-carbene complexes **15M**–**18M** (Table 1). The most stable of all the *N*-protonated quinolylidene and isoquinolylidene complexes are the *abnormal* isomers **18M** where the N–H group is closest to the carbene carbon atom. A similar situation is also found for the *N*-methylated complexes **11M**–**14M** and **19M**–**22M** except that complexes **22M**, which are the methylated analogue of the protonated complexes **18M**, are now the *least* stable isomers. We believe that compounds **22M** are destabilized by steric repulsion between the methyl group and the metal fragment at the α position of the annelated benzene ring. The most stable *N*-methylated complex is thus the *normal* **12M**, showing that remoteness is not necessarily disadvantageous with respect to the overall stability although such a statement could apply more to the free ligands. Note that the most stable of all the *N*-protonated quinolylidene and isoquinolylidene complexes, **18M**, possesses the *longest* metal–ligand bonds for all metals in the isomer series **7M**–**10M** and **15M**–**18M** (Figure 6). In contrast, the energetically lowest-lying *N*-methylated isoquinolylidene complexes, **12M**, possess the *shortest* metal–ligand bonds of the isomers **11M**–**14M** and **19M**–**22M**.

The metal–ligand interactions induce a significant change in the relative energies of the complexes compared to those of the free ligands upon complexation. Table 1 shows that **18** is clearly the most stable isomer of the free ligands **7**–**10**, **15**–**18**. The difference becomes much smaller

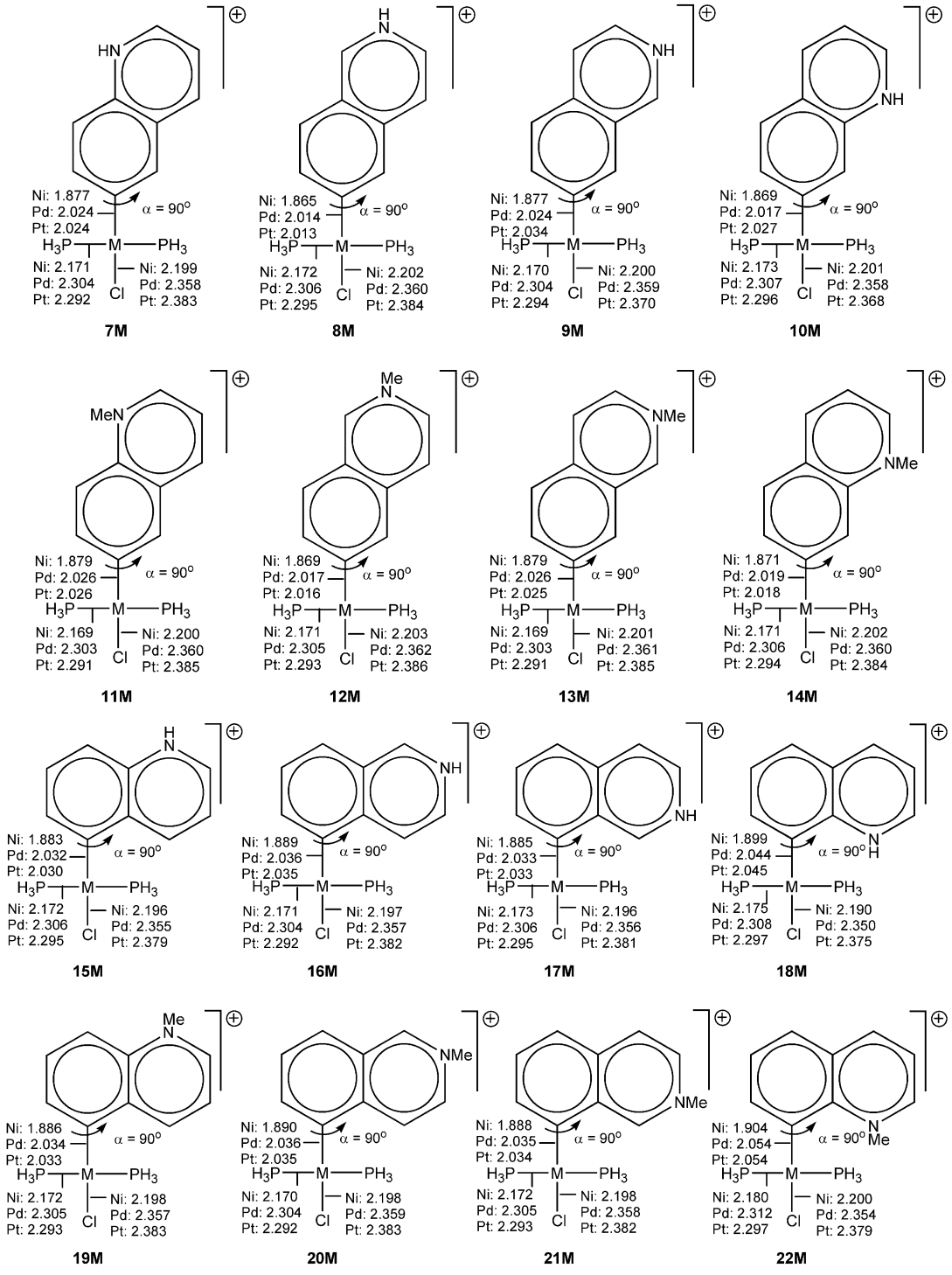

Figure 6. Schematic representation of the calculated quinolylidene and isoquinolylidene complexes 7**M**–**22M** (M = Ni, Pd, Pt). The optimised bond lengths for the M–$C_{carbene}$, M–PH_3 and M–Cl bonds are given in Å. The perpendicular arrangement of the ligands and the M$(PH_3)_2$Cl fragment is indicated by α.

in the respective complexes although **18M** is still the lowest-lying isomer of **7M**–**10M** and **15M**–**18M**. However, **18M** is also stabilized by intramolecular interactions between the N–H bond and the metal fragment. Inspection of the optimized geometry reveals that the N–H bond is clearly tilted toward the metal. A complete change in the stability order after complexation is calculated for the ligands **11**–**13** and **18**–**22** where the most stable free ligand **22** leads to the least stable complex **22M**, due to steric repulsion. The strongest metal–ligand bonding is calculated for **12M**. The main reason for these results will be discussed in the section on bonding analysis.

Finally we present the geometries and relative energies of the metal complexes **23M** and **24M** with the isomeric forms

of the imidazolylidene ligands. The most important bond lengths are given in Figure 7. The metal–carbene bond lengths in these complexes are nearly identical to certain six-membered pyridylidene complexes, e.g. **4M** and **5M** (Figure 5). The theoretically predicted relative stabilities of the isomeric complexes **23M** and **24M** show the expected order **23M** > **24M**. The strength and the nature of the metal–ligand bonding are discussed in the following section.

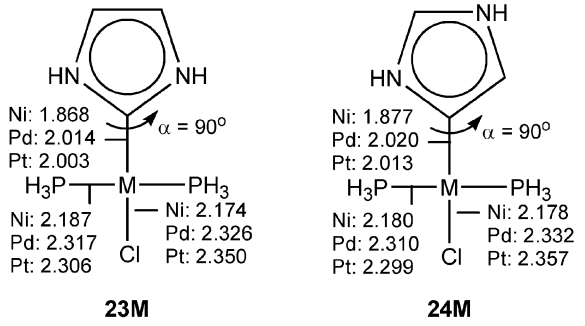

Figure 7. Schematic representation of the calculated imidazolylidene complexes **23M** and **24M** (M = Ni, Pd, Pt). The optimised bond lengths for the M–$C_{carbene}$, M–PH_3 and M–Cl bonds are given in Å.The perpendicular arrangement of the ligands and the $M(PH_3)_2Cl$ fragment is indicated by α.

Bonding Analysis

Tables 2 and 3 show the EDA results for the complexes **1M**–**6M**. The interacting fragments of the neutral complexes **1M**–**3M** are the charged closed-shell species $M(PH_3)_2Cl^+$ and the *ortho*, *meta* and *para* pyridyl anions. The interacting fragments of the cationic complexes **4M**–**6M** are the same $M(PH_3)_2Cl^+$ fragment and the neutral pyridylidenes.

The EDA results for the neutral complexes **1M**–**3M** show that the *ortho* complexes **1M** have bond dissociation energies D_e which are ca. 10 kcal/mol higher than for the *meta* and *para* complexes **2M** and **3M** which possess very similar values. This is in agreement with the change in the relative stability of the *ortho*, *meta* and *para* isomers after complexation, which was discussed above. Note that the differences between the BDE values given in Table 2, Table 3 do not exactly agree with the change in the stability order shown in Table 1 because the former values are subject to the basis set superposition error (BSSE). The differences between the two sets of data are small, however (< 1 kcal/mol in most cases).

The data in Tables 2 and 3 show also that the ΔE_{prep} values, which give the energy relaxation of the fragments from the geometry in the complex to the equilibrium values of the isolated fragments, are not very large and that the differences between the *ortho*, *meta* and *para* isomers are quite small. This means that the intrinsic interaction energies ΔE_{int} may also be used to elucidate the differences between the metal–ligand interactions of the isomers and the order of the ΔE_{int} values for the *ortho*, *meta* and *para* isomers is always the same as the order of the D_e values. The breakdown of the ΔE_{int} values into the electrostatic attraction ΔE_{elstat} and the orbital term ΔE_{orb} indicates that the bonding is dominated by the former term which contributes ca. 74% to the total attraction in the neutral complexes and ca. 68% in the charged complexes. The relative contributions of electrostatic attraction and orbital interactions do not significantly change between the *ortho*, *meta* and *para* isomers. The absolute ΔE_{int} values of the neutral pyridyl complexes **1M**–**3M** are much higher than those of the cationic carbene complexes **4M**–**6M** because the interacting fragments in the former species are cations and anions while in the latter cations and a neutral fragments interact.

What is the difference in the nature of the metal–carbon bond between the *ortho* (*normal*) isomers, where the nitrogen atom is adjacent to the ipso carbon atom, and the remote complexes which are the *meta* (*abnormal*) and *para* (*normal*) isomers? Which factors are responsible for the peculiar trend in the relative stability and BDE of the isomeric complexes? We first discuss the EDA results of the carbene precursor complexes **1M**–**3M**. Table 2 shows that the attractive contributions of ΔE_{orb} and particularly ΔE_{elstat} but

Table 2. Energy decomposition analysis at the BP86/TZ2P level for pyridyl complexes **1M**–**3M**. The complexes were split into a cationic metal fragment $[M(PH_3)_2Cl]^+$ and the anionic pyridyl ligands. Energy values in [kcal/mol].

	1Ni	**2Ni**	**3Ni**	**1Pd**	**2Pd**	**3Pd**	**1Pt**	**2Pt**	**3Pt**
ΔE_{int}	–226.2	–212.7	–213.8	–221.9	–209.1	–209.2	–232.3	–220.6	–219.8
ΔE_{Pauli}	219.5	202.9	210.9	239.6	225.8	228.5	296.9	281.7	281.7
ΔE_{elstat}[a]	–325.2 (73.0%)	–306.3 (73.7%)	–309.5 (72.9%)	–346.0 (75.0%)	–326.8 (77.1%)	–326.7 (74.6%)	–400.1 (75.6%)	–379.3 (75.5%)	–377.1 (75.2%)
ΔE_{orb}[a]	–120.5 (27.0%)	–109.3 (26.3%)	–115.2 (27.1%)	–115.5 (25.0%)	–108.0 (22.9%)	–111.0 (25.4%)	–129.1 (24.4%)	–123.0 (24.5%)	–124.5 (24.8%)
ΔE_{σ} (a′)[b]	–101.7 (84.4%)	–93.0 (85.1%)	–96.8 (84.0%)	–101.0 (87.5%)	–94.4 (87.4%)	–96.2 (86.7%)	–113.7 (88.0%)	–108.4 (88.1%)	–109.0 (87.6%)
ΔE_{π} (a″)[b]	–18.8 (15.6%)	–16.2 (14.9%)	–18.4 (16.0%)	–14.4 (12.5%)	–13.6 (12.6%)	–14.8 (13.3%)	–15.4 (12.0%)	–14.7 (11.9%)	–15.5 (12.4%)
ΔE_{prep}	8.5	6.5	6.0	9.6	7.1	7.0	9.4	7.4	6.6
ΔE (= $-D_e$)	–217.6	–206.2	–207.9	–212.3	–202.0	–202.2	–222.9	–213.2	–213.2

[a] The percentage values in parentheses give the contribution to the total attractive interactions ΔE_{elstat} + ΔE_{orb}. [b] The percentage values in parentheses give the contribution to the total orbital interactions ΔE_{orb}.

Table 3. Energy decomposition analysis at the BP86/TZ2P level for pyridylidene complexes **4M**–**6M**. The complexes were split into a cationic metal fragment $[M(PH_3)_2Cl]^+$ and the neutral carbene ligands. Energy values in [kcal/mol].

	4Ni	**5Ni**	**6Ni**	**4Pd**	**5Pd**	**6Pd**	**4Pt**	**5Pt**	**6Pt**
ΔE_{int}	–100.3	–108.5	–112.9	–94.8	–103.1	–106.6	–110.1	–117.8	–120.9
ΔE_{Pauli}	161.6	161.2	176.4	176.6	175.0	188.4	231.0	227.4	241.3
ΔE_{elstat}[a]	–179.8	–184.4	–196.9	–191.0	–195.3	–207.1	–240.7	–242.8	–255.3
	(68.6%)	(68.4%)	(68.1%)	(70.4%)	(70.2%)	(70.2%)	(70.6%)	(70.4%)	(70.5%)
ΔE_{orb}[a]	–82.2	–85.3	–92.3	–80.3	–82.8	–87.9	–100.4	–102.3	–106.9
	(31.4%)	(31.6%)	(31.9%)	(29.6%)	(29.8%)	(29.8%)	(29.4%)	(29.6%)	(29.5%)
ΔE_{σ} (a′)[b]	–66.1	–70.3	–72.5	–66.7	–70.2	–72.7	–84.3	–87.5	–89.4
	(80.5%)	(82.3%)	(79.4%)	(83.1%)	(84.8%)	(82.7%)	(84.0%)	(85.5%)	(84.3%)
ΔE_{π} (a″)[b]	–16.0	–15.1	–18.8	–13.6	–12.6	–15.2	–16.1	–14.8	–16.6
	(19.5%)	(17.7%)	(20.6%)	(16.9%)	(15.2%)	(17.3%)	(16.0%)	(14.5%)	(15.7%)
ΔE_{prep}	3.4	3.4	2.9	3.0	2.9	2.6	4.5	4.5	3.5
ΔE (= $-D_e$)	–96.9	–105.1	–110.0	–91.8	–100.2	–104.0	–105.6	–113.3	–117.4

[a] The percentage values in parentheses give the contribution to the total attractive interactions $\Delta E_{elstat} + \Delta E_{orb}$. [b] The percentage values in parentheses give the contribution to the total orbital interactions ΔE_{orb}.

also the repulsive term ΔE_{Pauli} are larger in the *ortho* isomers **1M** than in the *meta* and *para* forms **2M** and **3M**. The electrostatic attraction comes mainly from the overlap of the σ-electron pair of the ligand with the nucleus of the metal atom.[34] The σ-electron pair orbital is also the major contributor to the ΔE_{σ} ((a′)) term which forms the largest part of the orbital term ΔE_{orb} (Table 2). In comparison, the π-orbital term ΔE_{π} (a″) is much smaller and shows much less variation between the *ortho*, *meta* and *para* complexes. The very small differences between the ΔE_{π} (a″) values of **1M** and **3M** clearly show that the variation in the rotational barriers are *not* caused by stronger π-bonding in the latter species which may rather be due to steric interactions. The data further suggest that the σ lone-pair orbital plays a pivotal role in the observed trend of the stabilities and metal–ligand bond strengths.

The EDA results for the cationic pyridylidene complexes **4M**–**6M** show that the strongest metal–ligand interactions are found in the remote *para* complexes **6M** (Table 3). This is different from the neutral complexes where the metal–ligand interactions are the strongest in the *ortho* complexes **1M**. The differences between the ΔE_{prep} values of **4M**–**6M** are very small and thus, the differences in bonding between the isomers can be discussed by examination of the ΔE_{int} values which show the trend **4M** < **5M** < **6M**. The latter trend is mainly determined by ΔE_{elstat} and ΔE_{orb} where the σ contribution dominates the orbital interactions. Note that the ΔE_{π} (a″) interactions make only a small contribution to the stronger ΔE_{int} values of the *para* complexes **6M**. However, comparison of the relatively weak π-contributions within the series shows a consistent trend, i.e. *the normal ortho* and *para* carbenes in **4M** and **6M** are better π-acceptors than the *abnormal meta* isomers in **5M**.

The EDA result for the *N*-protonated quinolylidene and isoquinolylidene complexes **7M**–**10M** and their *N*-methylated homologues **11M**–**14M** where the metal fragment is bonded to a carbene carbon atom in a β-position to the annelated benzene ring, are shown in Tables 4, 5 and 6. It becomes obvious that the strength and the nature of the metal–ligand interactions vary very little within the three series of compounds. The complexes **12M** have the strongest metal–ligand bonds but the differences with respect to

Table 4. Energy decomposition analysis at the BP86/TZ2P level for the protonated (**7Ni**–**10Ni**) and methylated (**11Ni**–**14Ni**) Ni-(iso)-quinolylidene complexes. The complexes were split into a positive fragment $Ni(PH_3)_2Cl^+$ and a neutral fragment consisting of the carbene ligand. Energy values in [kcal/mol].

	7Ni	**8Ni**	**9Ni**	**10Ni**	**11Ni**	**12Ni**	**13Ni**	**14Ni**
ΔE_{int}	–127.1	–128.6	–127.7	–124.9	–129.1	–130.8	–130.0	–126.8
ΔE_{Pauli}	174.3	179.4	174.2	176.0	174.6	178.8	174.9	178.0
ΔE_{elstat}[a]	–207.1	–211.9	–207.4	–206.4	–209.6	–213.3	–210.2	–209.6
	(68.7%)	(68.8%)	(68.7%)	(68.6%)	(69.0%)	(68.9%)	(68.9%)	(68.8%)
ΔE_{orb}[a]	–94.3	–96.0	–94.5	–94.5	–94.1	–96.4	–94.7	–95.2
	(31.3%)	(31.2%)	(31.3%)	(31.4%)	(31.0%)	(31.1%)	(31.1%)	(31.2%)
ΔE_{σ} (a′)[b]	–75.9	–76.1	–76.3	–75.1	–75.9	–76.4	–76.4	–75.8
	(80.5%)	(79.2%)	(80.7%)	(79.5%)	(80.6%)	(79.3%)	(80.6%)	(79.6%)
ΔE_{π} (a″)[b]	–18.4	–20.0	–18.2	–19.4	–18.3	–20.0	–18.4	–19.4
	(19.5%)	(20.8%)	(19.3%)	(20.5%)	(19.4%)	(20.7%)	(19.4%)	(20.4%)
ΔE_{prep}	4.1	4.1	4.2	4.0	4.3	4.3	4.3	4.1
ΔE (= $-D_e$)	–123.0	–124.5	–123.5	–120.8	–124.8	–126.6	–125.7	–122.7

[a] The percentage values in parentheses give the contribution to the total attractive interactions $\Delta E_{elstat} + \Delta E_{orb}$. [b] The percentage values in parentheses give the contribution to the total orbital interactions ΔE_{orb}.

Table 5. Energy decomposition analysis at the BP86/TZ2P level for the protonated (**7Pd**–**10Pd**) and methylated (**11Pd**–**14Pd**) Pd-(iso)-quinolylidene complexes. The complexes were split into a positive fragment $Pd(PH_3)_2Cl^+$ and a neutral fragment consisting of the carbene ligand. Energy values in [kcal/mol].

	7Pd	**8Pd**	**9Pd**	**10Pd**	**11Pd**	**12Pd**	**13Pd**	**14Pd**
ΔE_{int}	–121.6	–122.8	–122.2	–119.1	–123.8	–125.1	–124.7	–121.1
ΔE_{Pauli}	189.3	195.1	189.5	191.4	190.0	194.7	190.5	193.6
ΔE_{elstat}[a]	–219.1	–224.3	–219.6	–218.5	–222.0	–225.8	–222.7	–222.0
	(70.5%)	(70.6%)	(70.5%)	(70.4%)	(70.7%)	(70.6%)	(70.7%)	(70.5%)
ΔE_{orb}[a]	–91.8	–93.5	–92.1	–92.0	–91.8	–94.0	–92.5	–92.7
	(29.5%)	(29.4%)	(29.5%)	(29.6%)	(29.3%)	(29.4%)	(29.3%)	(29.5%)
ΔE_{σ} (a′)[b]	–76.2	–76.5	–76.6	–75.5	–76.2	–76.9	–76.7	–76.2
	(82.9%)	(81.9%)	(83.1%)	(82.1%)	(83.0%)	(81.9%)	(83.0%)	(82.2%)
ΔE_{π} (a′′)[b]	–15.7	–17.0	–15.5	–16.5	–15.6	–17.1	–15.8	–16.5
	(17.1%)	(18.1%)	(16.9%)	(17.9%)	(17.0%)	(18.1%)	(17.0%)	(17.8%)
ΔE_{prep}	3.9	4.0	4.0	3.8	4.2	4.1	4.2	4.0
ΔE (= $-D_e$)	–117.7	–118.8	–118.2	–115.3	–119.6	–121.0	–120.5	–117.2

[a] The percentage values in parentheses give the contribution to the total attractive interactions ΔE_{elstat} + ΔE_{orb}. [b] The percentage values in parentheses give the contribution to the total orbital interactions ΔE_{orb}.

Table 6. Energy decomposition analysis at the BP86/TZ2P level for the protonated (**7Pt**–**10Pt**) and methylated (**11Pt**–**14Pt**) Pt-(iso)-quinolylidene complexes. The complexes were split into a positive fragment $Pt(PH_3)_2Cl^+$ and a neutral fragment consisting of the carbene ligand. Energy values in [kcal/mol].

	7Pt	**8Pt**	**9Pt**	**10Pt**	**11Pt**	**12Pt**	**13Pt**	**14Pt**
ΔE_{int}	–135.8	–137.2	–134.8	–131.9	–137.8	–139.4	–138.7	–135.4
ΔE_{Pauli}	242.0	249.7	240.0	242.4	242.8	249.1	243.8	247.9
ΔE_{elstat}[a]	–267.7	–274.7	–264.9	–264.1	–270.7	–276.1	–271.9	–272.2
	(70.9%)	(71.0%)	(70.7%)	(70.6%)	(71.1%)	(71.1%)	(71.1%)	(71.0%)
ΔE_{orb}[a]	–110.1	–112.2	–110.0	–110.2	–109.9	–112.5	–110.6	–111.2
	(29.1%)	(29.0%)	(29.3%)	(29.4%)	(28.9%)	(28.9%)	(28.9%)	(29.0%)
ΔE_{σ} (a′)[b]	–92.6	–93.1	–92.4	–91.6	–92.5	–93.4	–93.1	–92.7
	(84.1%)	(83.0%)	(84.1%)	(83.1%)	(84.2%)	(83.1%)	(84.1%)	(83.4%)
ΔE_{π} (a′′)[b]	–17.5	–19.1	–17.5	–18.7	–17.4	–19.0	–17.5	–18.5
	(15.9%)	(17.0%)	(15.9%)	(16.9%)	(15.8%)	(16.9%)	(15.9%)	(16.6%)
ΔE_{prep}	5.3	5.3	4.6	4.3	5.5	5.4	5.5	5.3
ΔE (= $-D_e$)	–130.5	–131.9	–130.3	–127.6	–132.4	–134.0	–133.2	–130.2

[a] The percentage values in parentheses give the contribution to the total attractive interactions ΔE_{elstat} + ΔE_{orb}. [b] The percentage values in parentheses give the contribution to the total orbital interactions ΔE_{orb}.

the other complexes are not very large. Substitution of a proton in **7M**–**10M** by a methyl cation in **11M**–**14M** changes the metal–ligand bonding very little. We want to point out that the D_e values and the ΔE_{int} values of the quinolylidene and isoquinolylidene complexes **7M**–**14M** are 15 – 25 kcal/mol higher than the values of the pyridylidene complexes **4M**–**6M** which shows that the metal–ligand bonds in the former species are significantly stronger. Yet, the M–C bond lengths in **7M**–**14M** are very similar for the same metal. This is another indication that the bond length in donor–acceptor complexes is not a good indicator for bond strength. While the ΔE_{int} values of **7M**–**14M** are higher than in **4M**–**6M**, the nature of the bonding remains nearly the same. The percentage contribution of ΔE_{elstat} and ΔE_{orb} to ΔE_{int} and the relative contributions of ΔE_{σ} ((a′)) and ΔE_{π} ((a′′)) to ΔE_{orb} in the two sets of compounds do not differ much.

Tables 7, 8, and 9 show the EDA result for the *N*-protonated isoquinolylidene and quinolylidene complexes **15M**–**18M** and their *N*-methylated homologues **19M**–**22M** wherein the metal fragment is bonded to an α carbene carbon atom of the annelated benzene ring. The variation between the D_e values and the ΔE_{int} values is much larger than for the complexes **7M**–**14M**. It is useful to compare the EDA results of the protonated species **15M**–**18M** with the data for the isomers **7M**–**10M** which are given in Tables 4, 5, and 6. The calculated values for D_e and ΔE_{int} again clearly illustrates that the complexes **18M** have the weakest metal–ligand bond. It is not impossible that the α-proton, that seems to bent towards the metal, could be partly responsible for this result. Table 1 shows that the ligand **18** is the most stable isomer of the carbenes **7**–**10** and **15**–**18**. A similar situation is found for the free ligands **11**–**14** and **19**–**22** and complexes **11M**–**14M** and **19M**–**22M** of the *N*-methylated homologues. The most stable free ligand **22** (Table 1) has the weakest metal–ligand bonds in **22M** (Tables 7, 8, and 9). However for **22** and **22M** steric repulsion between a methyl group and the metal fragment exacerbate the general effect to afford the weakest metal ligand bond of all the complexes mentioned. The differences

Table 7. Energy decomposition analysis at the BP86/TZ2P level for the protonated (**15Ni**–**18Ni**) and methylated (**19Ni**–**22Ni**) Ni-(iso)-quinolylidene complexes. The complexes were split into a positive fragment $Ni(PH_3)_2Cl^+$ and a neutral fragment consisting of the carbene ligand. Energy values in [kcal/mol].

	15Ni	**16Ni**	**17Ni**	**18Ni**	**19Ni**	**20Ni**	**21Ni**	**22Ni**
ΔE_{int}	–120.0	–122.0	–119.2	–111.5	–122.2	–124.6	–121.3	–110.8
ΔE_{Pauli}	174.0	174.1	181.1	170.4	175.5	175.1	178.0	173.4
ΔE_{elstat}[a]	–200.6	–202.9	–206.5	–190.3	–203.9	–205.8	–204.8	–189.6
	(68.2%)	(68.5%)	(68.7%)	(67.5%)	(68.5%)	(68.6%)	(68.5%)	(66.7%)
ΔE_{orb}[a]	–93.4	–93.2	–93.9	–91.6	–93.7	–94.0	–94.4	–94.6
	(31.8%)	(31.5%)	(31.3%)	(32.5%)	(31.5%)	(31.4%)	(31.5%)	(33.3%)
ΔE_{σ} (a′)[b]	–76.5	–76.8	–76.6	–76.3	–76.5	–77.3	–77.3	–77.0
	(81.9%)	(82.4%)	(81.5%)	(83.3%)	(81.6%)	(82.2%)	(81.9%)	(81.4%)
ΔE_{π} (a″)[b]	–16.9	–16.4	–17.3	–15.3	–17.3	–16.7	–17.1	–17.6
	(18.1%)	(17.6%)	(18.5%)	(16.7%)	(18.4%)	(17.8%)	(18.1%)	(18.6%)
ΔE_{prep}	3.6	4.2	4.6	3.8	3.7	4.2	4.2	7.1
ΔE (= $-D_e$)	–116.4	–117.8	–114.6	–107.7	–118.5	–120.4	–117.1	–103.7

[a] The percentage values in parentheses give the contribution to the total attractive interactions ΔE_{elstat} + ΔE_{orb}. [b] The percentage values in parentheses give the contribution to the total orbital interactions ΔE_{orb}.

Table 8. Energy decomposition analysis at the BP86/TZ2P level for the protonated (**15Pd**–**18Pd**) and methylated (**19Pd**–**22Pd**) Pd-(iso)-quinolylidene complexes. The complexes were split into a positive fragment $Pd(PH_3)_2Cl^+$ and a neutral fragment consisting of the carbene ligand. Energy values in [kcal/mol].

	15Pd	**16Pd**	**17Pd**	**18Pd**	**19Pd**	**20Pd**	**21Pd**	**22Pd**
ΔE_{int}	–114.8	–117.0	–114.0	–107.3	–117.0	–119.7	–116.4	–104.4
ΔE_{Pauli}	187.5	188.2	190.8	185.7	189.3	189.7	192.0	180.2
ΔE_{elstat}[a]	–212.1	–214.9	–214.8	–204.4	–215.6	–218.2	–217.0	–195.1
	(70.1%)	(70.4%)	(70.5%)	(69.8%)	(70.4%)	(70.5%)	(70.4%)	(68.6%)
ΔE_{orb}[a]	–90.2	–90.3	–90.0	–88.6	–90.7	–91.2	–91.3	–89.5
	(29.9%)	(29.6%)	(29.5%)	(30.2%)	(29.6%)	(29.5%)	(29.6%)	(31.4%)
ΔE_{σ} (a′)[b]	–76.0	–76.3	–75.6	–75.4	–76.1	–76.9	–76.8	–75.0
	(84.2%)	(84.6%)	(84.0%)	(85.1%)	(83.9%)	(84.4%)	(84.1%)	(83.8%)
ΔE_{π} (a″)[b]	–14.3	–13.9	–14.4	–13.2	–14.6	–14.3	–14.5	–14.5
	(15.8%)	(15.4%)	(16.0%)	(14.9%)	(16.1%)	(15.6%)	(15.9%)	(16.2%)
ΔE_{prep}	2.7	4.0	4.3	3.8	3.6	4.3	4.5	6.7
ΔE (= $-D_e$)	–112.1	–113.0	–109.7	–103.5	–113.4	–115.4	–111.9	–97.7

[a] The percentage values in parentheses give the contribution to the total attractive interactions ΔE_{elstat} + ΔE_{orb}. [b] The percentage values in parentheses give the contribution to the total orbital interactions ΔE_{orb}.

Table 9. Energy decomposition analysis at the BP86/TZ2P level for the protonated (**15Pt**–**18Pt**) and methylated (**19Pt**–**22Pt**) Pt-(iso)-quinolylidene complexes. The complexes were split into a positive fragment $Pt(PH_3)_2Cl^+$ and a neutral fragment consisting of the carbene ligand. Energy values in [kcal/mol].

	15Pt	**16Pt**	**17Pt**	**18Pt**	**19Pt**	**20Pt**	**21Pt**	**22Pt**
ΔE_{int}	–128.9	–131.0	–128.1	–121.9	–131.1	–133.5	–130.3	–117.7
ΔE_{Pauli}	241.1	240.9	244.4	239.3	242.1	242.5	245.5	230.3
ΔE_{elstat}[a]	–261.0	–263.4	–264.1	–253.5	–264.3	–266.8	–266.3	–240.7
	(70.6%)	(70.8%)	(70.9%)	(70.2%)	(70.8%)	(71.0%)	(70.9%)	(69.1%)
ΔE_{orb}[a]	–108.9	–108.5	–108.4	–107.8	–109.0	–109.2	–109.5	–107.4
	(29.4%)	(29.2%)	(29.1%)	(29.8%)	(29.2%)	(29.0%)	(29.1%)	(30.8%)
ΔE_{σ} (a′)[b]	–92.8	–92.9	–92.2	–93.1	–92.6	–93.3	–93.3	–91.3
	(85.2%)	(85.6%)	(85.1%)	(86.4%)	(85.0%)	(85.4%)	(85.2%)	(85.0%)
ΔE_{π} (a″)[b]	–16.1	–15.6	–16.1	–14.7	–16.4	–15.9	–16.2	–16.1
	(14.8%)	(14.4%)	(14.9%)	(13.6%)	(15.0%)	(14.6%)	(14.8%)	(15.0%)
ΔE_{prep}	4.6	5.2	5.4	4.9	5.0	5.4	5.5	6.7
ΔE (= $-D_e$)	–124.3	–125.8	–122.7	–117.0	–126.1	–128.1	–124.8	–111.0

[a] The percentage values in parentheses give the contribution to the total attractive interactions ΔE_{elstat} + ΔE_{orb}. [b] The percentage values in parentheses give the contribution to the total orbital interactions ΔE_{orb}.

between the D_e and ΔE_{int} values of the other complexes are much smaller and so are the differences between the relative energies of the free ligands. Note that for all complexes **1M**–**22M** holds that the metal–ligand bond strength has the order for the three metals Pt > Ni > Pd which is the well-known V-shaped trend for elements of the three transition

Table 10. Energy decomposition analysis at the BP86/TZ2P level for group-10 complexes containing the ligands **23** and **24**. The complexes were split into a positive fragment $Pt(PH_3)_2Cl^+$ and a neutral fragment consisting of the carbene ligand. Energy values in [kcal/mol].

	23Ni	**24Ni**	**23Pd**	**24Pd**	**23Pt**	**24Pt**
ΔE_{int}	–90.9	–101.7	–85.9	–96.8	–101.1	–111.5
ΔE_{Pauli}	147.9	151.4	161.7	165.9	215.3	218.0
ΔE_{elstat}[a]	–164.5	–174.6	–174.9	–186.1	–222.8	–232.7
	(68.9%)	(69.0%)	(70.6%)	(70.8%)	(70.4%)	(70.6%)
ΔE_{orb}[a]	–74.3	–78.5	–72.7	–76.6	–93.6	–96.8
	(31.1%)	(31.0%)	(29.4%)	(29.2%)	(29.6%)	(29.4%)
ΔE_{σ} (a′)[b]	–60.8	–65.5	–61.1	–65.5	–79.4	–83.6
	(81.8%)	(83.4%)	(84.0%)	(85.5%)	(84.8%)	(86.3%)
ΔE_{π} (a′′)[b]	–13.5	–13.0	–11.6	–11.1	–14.2	–13.2
	(18.2%)	(16.6%)	(16.0%)	(14.5%)	(15.2%)	(13.7%)
ΔE_{prep}	2.8	3.1	2.4	2.8	3.9	4.2
ΔE (= $-D_e$)	–88.1	–98.6	–83.5	–94.0	–97.2	–107.3

[a] The percentage values in parentheses give the contribution to the total attractive interactions $\Delta E_{elstat} + \Delta E_{orb}$. [b] The percentage values in parentheses give the contribution to the total orbital interactions ΔE_{orb}.

metal rows.[35] An interesting observation is made when one compares the nature of the metal-carbene bonding in **7M**–**14M** with the EDA values for **15M**–**22M**. The relative contributions of ΔE_{elstat} and ΔE_{orb} to ΔE_{int} are very similar to each other but the orbital interactions in the α-carbene complexes **15M**–**22M** have uniformly a slightly lower π-bonding character than the β-carbene complexes **7M**–**14M**. This becomes obvious by the percentage contributions of ΔE_{π} (a′′) to ΔE_{orb} in the two sets of compounds.

Finally we present the EDA results for the group-10 complexes with the isomeric two-N, five-membered heterocyclic ligands **23M** and **24M**, the first a *normal* and the second an *abnormal* carbene complex. The data are given in Table 10. The calculated results for D_e and ΔE_{int} show that **23M** is weaker bonded than **24M**. The same sequence has previously been calculated for complexes where M is a transition metal of groups 4, 6, 8, 10 in the periodic system.[13] The present results show that the nature of the metal–carbene bonding in imidazolylidenes is rather similar to that in the complexes **4M**–**22M**.

The energy-decomposition analysis of the metal–ligand bonds indicates that the percentage contributions of the EDA terms do not change a lot. So which factor determines the differences and the trend in the strength of the metal–ligand interactions? This is discussed in the following section.

Discussion

The EDA results suggest that the σ lone-pair donor orbital of the carbene ligands plays a pivotal role in the strength of the metal–ligand interactions and that the π-contribution is less important for the bonding. This is not a new result, it has been suggested in most previous studies[12a–12o] except for two reports which say that π interactions in NHC complexes may be significant.[12p,12q] What is surprising in the present finding is that the general nature of the bonding hardly changes when the nitrogen atom in the heterocyclic carbene is in the *ortho*, *meta* or *para* position or if it occurs in an adjacent ring of the (iso)quinolylidene ligand. We want to point out that the σ lone-pair electrons of the ligand do not only yield the main part of the orbital interactions, they also make the largest contribution to the electrostatic term because they interact strongly with the metal nucleus. Therefore, we considered the σ lone-pair orbital of the heterocyclic ligands which are the highest occupied MO of the molecules. Table 1 give the energy levels ε(HOMO) of **1**–**24**.

The HOMOs of the free pyridyl groups (carbeniates) **1**–**3** are as expected energetically higher lying than the HOMOs of the neutral pyridylidene ligands **4**–**6** (Table 1). More interesting is the trend of ε(HOMO). The anions **1**–**3** show for ε(HOMO) the order *ortho* > *meta* > *para*, i.e. the *ortho* isomer **1** has the highest lying HOMO while the *para* isomer **3** has the lowest lying HOMO. The opposite order is calculated for the carbenes **4**–**6**. For both sets of compounds we calculate the order *ortho* < *meta* < *para*, i.e. the *ortho* isomer has the lowest lying HOMO while the *para* isomer has the highest lying HOMO. These results are in agreement with the trend of the ΔE_{int} values of all the complexes **1M**–**6M** (Tables 2, 3). Remarkably, a linear relationship is obtained when calculated ΔE_{int} values of a chosen metal in the full series **1M**–**22M** are plotted against the ε(HOMO) values of the ligands (carbeniate and carbene) **1**–**22**. The importance of this relationship seemingly even overrides repulsion effects as was pointed out for **22M** before.

Figure 8 (a–c), exhibit the best-fit lines which, for all metals, have correlation coefficients >0.99. Note that the ε(HOMO) values of the (iso)quinolylidene ligands **7**–**22** exhibit the same trend as the pyridinium derived carbenes **4**–**6**, but the differences in the absolute values are smaller because the nitrogen atom in the former species is in the adjacent ring while in the latter carbenes it is in the same ring. The pivotal role of the carbene σ lone-pair orbital for the trend of the metal–ligand bond strength comes clearly to the fore by the EDA results and the correlations shown in Figure 8. An energetically higher lying σ lone-pair orbital yields stronger orbital interactions because (a) the HOMO–LUMO gap with the LUMO of the metal fragment is

smaller and, (b) there is stronger electrostatic attraction which comes from the better overlap with the nucleus of the metal atom. The latter can be explained with the hybridization of the σ lone-pair orbital which has a higher %p character in the energetically higher lying carbenes.

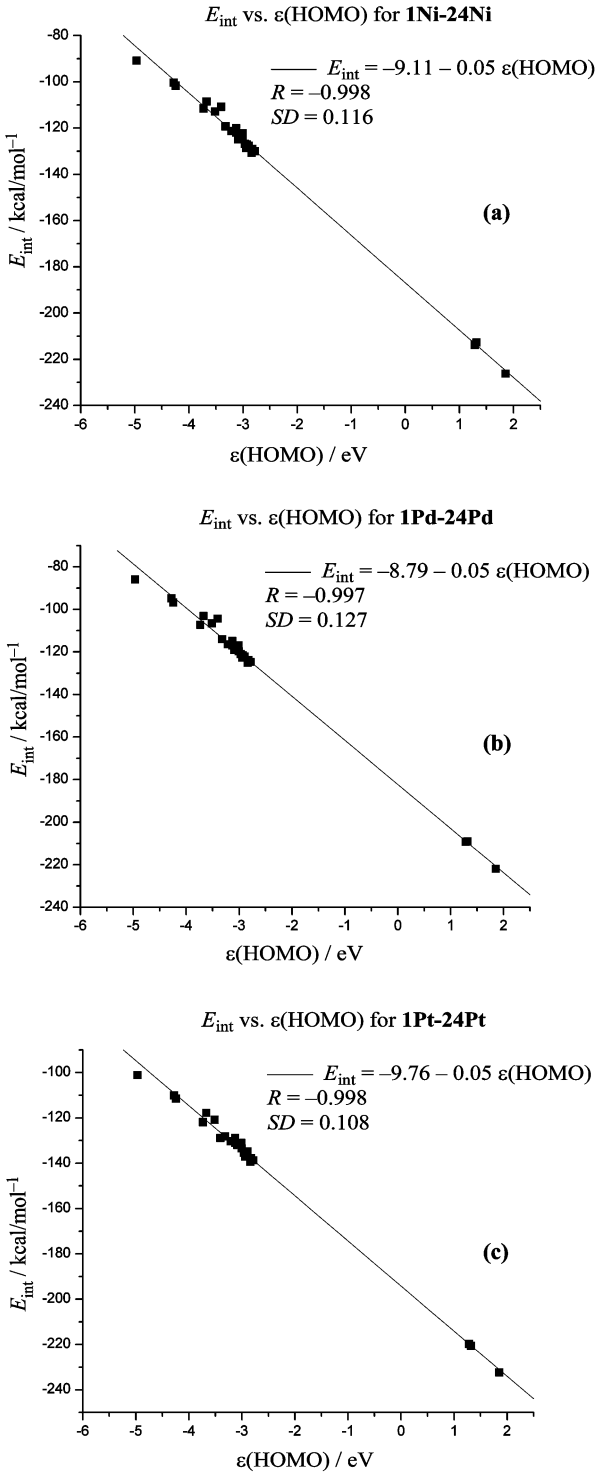

Figure 8. Correlation between ε(HOMO) of the free ligands **1**–**24** and the metal–ligand interaction energies ΔE_{int} in the corresponding complexes **1M**–**24M**. M = (a) Ni, (b) Pd, (c) Pt.

Summary

The results of this work can be summarized as follows. The EDA results suggest that the nature of the metal–carbene bonds in the complexes **4M**–**22M** shows little variation when the position of the nitrogen atom is *adjacent* (*ortho*) or *remote* (*meta* or *para*). It changes also very little when the nitrogen atom is in an adjacent ring to the cyclic carbene moiety. The most significant differences between the bond strengths come from the energy level of the σ HOMO of the carbene ligand which depends a lot on the position of the nitrogen atom. This holds also for the two isomers of the five-membered N-heterocyclic carbenes. An energetically higher-lying σ lone-pair orbital of the carbene ligand yields stronger orbital interactions but also stronger electrostatic attraction because of better interaction with the metal nucleus. There is an excellent correlation between the ε(HOMO) values of the ligands and the metal–ligand interaction energies, ΔE_{int}.

Supporting Information (see also the footnote on the first page of this article): Table 1S gives the Cartesian coordinates and the total energies of all calculated structures.

Acknowledgments

The authors thank the computer centre Marburg for the excellent service and computational time provided. G. H. thanks the National Research Foundation of South Africa (Grant number SFP2005110900004) and the Deutscher Akademischer Austauschdienst (DAAD) (Grant number A/05/52686) for post-doctoral funding. O. S. was supported by the Alexander von Humboldt Foundation and the German Academy of Sciences Leopoldina (BMBF LPD 9901/8-179). G. F. thanks the Deutsche Forschungsgemeinschaft (DFG) for financial support.

[1] A. J. Arduengo, R. L. Harlow, M. Kline, *J. Am. Chem. Soc.* **1991**, *113*, 361.
[2] Reviews: a) D. Bourissou, O. Guerret, F. Gabbaï, G. Bertrand, *Chem. Rev.* **2000**, *100*, 39; b) W. A. Herrmann, *Angew. Chem.* **2002**, *114*, 1342; *Angew. Chem. Int. Ed.* **2002**, *41*, 1290; c) T. Weskamp, V. P. W. Böhm, W. A. Herrmann, *J. Organomet. Chem.* **2000**, *600*, 12; d) C. M. Crudden, D. P. Allen, *Coord. Chem. Rev.* **2004**, *248*, 2247; e) *N-Heterocyclic Carbenes in Synthesis* (Ed.: S. P. Nolan), Wiley-VCH, Weinheim, **2006**; f) F. A. Glorius, *Top. Organomet. Chem.* **2007**, *21*, 1; g) A. C. Hillier, G. A. Grasa, M. S. Viciu, H. M. Lee, C. Yang, S. P. Nolan, *J. Organomet. Chem.* **2002**, *653*, 69; h) E. A. B. Kantchev, C. J. O'Brien, M. G. Organ, *Angew. Chem.* **2007**, *119*, 2824; *Angew. Chem. Int. Ed.* **2007**, *46*, 2768; i) F. E. Hahn, M. C. Jahnke, *Angew. Chem. Int. Ed.* **2008**, *47*, 3122.
[3] O. Schuster, L. Yang, H. G. Raubenheimer, M. Albrecht, *Chem. Rev.* **2009**, accepted for publication.
[4] H. G. Raubenheimer, J. G. Toerien, G. J. Kruger, R. Otte, W. van Zyl, P. Olivier, *J. Organomet. Chem.* **1994**, *466*, 291.
[5] S. K. Schneider, G. R. Julius, C. Loschen, H. G. Raubenheimer, G. Frenking, W. A. Herrmann, *Dalton Trans.* **2006**, 1226.
[6] S. K. Schneider, P. Roembke, G. R. Julius, H. G. Raubenheimer, W. A. Herrmann, *Adv. Synth. Catal.* **2006**, *348*, 1862; S. K. Schneider, C. F. Rentzsch, A. Krueger, H. G. Raubenheimer, W. A. Herrmann, *J. Mol. Catal. A* **2007**, *265*, 50.
[7] H. G. Raubenheimer, S. Cronje, *Dalton Trans.* **2008**, 1265.
[8] C. Strasser, E. Stander, O. Schuster, S. Cronje, H. G. Raubenheimer, *Eur. J. Inorg. Chem.* **2009**, this issue.

[9] W. H. Meyer, M. Deetlefs, M. Pohlmann, R. Scholz, M. W. Esterhuysen, G. R. Julius, H. G. Raubenheimer, *Dalton Trans.* **2004**, 413.
[10] S. K. Schneider, P. Roembke, G. R. Julius, C. Loschen, H. G. Raubenheimer, G. Frenking, W. A. Herrmann, *Eur. J. Inorg. Chem.* **2005**, 2973.
[11] O. Schuster, H. G. Raubenheimer, *Inorg. Chem.* **2006**, *45*, 7997.
[12] a) C. Boehme, G. Frenking, *Organometallics* **1998**, *17*, 5801; b) D. S. McGuiness, K. J. Cavell, B. W. Skelton, A. H. White, *Organometallics* **1999**, *18*, 1596; c) T. Weskamp, F. J. Kohl, W. Hieringer, D. Gleich, W. A. Herrmann, *Angew. Chem.* **1999**, *111*, 2573; *Angew. Chem. Int. Ed.* **1999**, *38*, 2416; d) J. Schwarz, V. P. W. Böhm, M. G. Gardiner, M. Grosche, W. A. Hermann, W. Hieringer, G. Raudaschl-Sieber, *Chem. Eur. J.* **2000**, *6*, 1773; e) L. Perrin, E. Clot, O. Eisenstein, J. Loch, R. H. Crabtree, *Inorg. Chem.* **2001**, *40*, 5806; f) A. A. D. Tulloch, A. A. Danopoulos, S. Kleinhenz, M. E. Light, M. B. Hursthouse, G. Eastham, *Organometallics* **2001**, *20*, 2027; g) D. V. Deubel, *Organometallics* **2002**, *21*, 4303; h) A. T. Termaten, M. Schakel, A. W. Ehlers, M. Lutz, A. L. Spek, K. Lammertsma, *Chem. Eur. J.* **2003**, *9*, 3577; i) X. Hu, Y. Tang, P. Gantzel, K. Meyer, *Organometallics* **2003**, *22*, 612; j) X. Hu, I. Castro-Rodriguez, K. Olsen, K. Meyer, *Organometallics* **2004**, *23*, 755; k) D. Nemcsok, K. Wichmann, G. Frenking, *Organometallics* **2004**, *23*, 3640; l) R. Dorta, E. D. Stevens, N. M. Scott, C. Costabile, L. Cavallo, C. D. Hoff, S. P. Nolan, *J. Am. Chem. Soc.* **2005**, *127*, 2485; m) N. M. Scott, R. Dorta, E. D. Stevens, A. Correa, L. Cavallo, S. P. Nolan, *J. Am. Chem. Soc.* **2005**, *127*, 3516; n) M. D. Sanderson, J. W. Kamplain, C. W. Bielawski, *J. Am. Chem. Soc.* **2006**, *128*, 16514; o) H. Jacobsen, A. Correa, C. Costabile, C. L. Cavallo, *J. Organomet. Chem.* **2006**, *691*, 4350; p) S. Diez-Gonzalez, S. P. Nolan, *Coord. Chem. Rev.* **2007**, *251*, 874; q) D. M. Khramov, V. M. Lynch, C. W. Bielawski, *Organometallics* **2007**, *26*, 6042; r) R. A. Kelly, H. Clavier, S. Giudice, N. M. Scott, E. D. Stevens, J. Bordner, I. Samardjiev, C. D. Hoff, L. Cavallo, S. P. Nolan, *Organometallics* **2008**, *27*, 202; s) A. Kausamo, H. M. Tuononen, K. E. Krahulic, R. Roesler, *Inorg. Chem.* **2008**, *47*, 1145; t) U. Radius, F. M. Bickelhaupt, *Organometallics* **2008**, *27*, 3410.
[13] R. Tonner, G. Heydenrych, G. Frenking, *Chem. Asian J.* **2007**, *2*, 1555.
[14] M. F. J. Lappert, *J. Organomet. Chem.* **1975**, *100*, 139.
[15] M. F. J. Lappert, *J. Chem. Soc., Dalton Trans.* **1977**, 2172.
[16] R. Dorta, E. D. Stevens, N. M. Scott, C. Costabile, L. Cavalo, C. D. Hoff, S. P. Nolan, *J. Am. Chem. Soc.* **2005**, *127*, 2485.
[17] N. Fröhlich, U. Pidun, M. Stahl, G. Frenking, *Organometallics* **1997**, *16*, 442.
[18] M.-T. Lee, C.-H. Hu, *Organometallics* **2004**, *23*, 976.
[19] C. Boehme, G. Frenking, *J. Am. Chem. Soc.* **1996**, *118*, 2039.
[20] A. C. Hillier, W. J. Sommer, B. S. Yong, J. L. Petersen, L. Cavallo, S. P. Nolan, *Organometallics* **2003**, *22*, 4322.
[21] R. H. Crabtree, *J. Organomet. Chem.* **2005**, *690*, 5451.
[22] D. J. Lavorato, J. K. Terlouw, G. A. McGibbon, T. K. Dargel, W. Koch, H. Schwarz, *Int. J. Mass Spectrom.* **1998**, *179/180*, 7.
[23] a) A. D. Becke, *Phys. Rev. A* **1988**, *38*, 3098; b) J. P. Perdew, *Phys. Rev. B* **1986**, *34*, 7406.
[24] J. G. Snijders, E. J. Baerends, P. Vernooijs, *At. Data Nucl. Data Tables* **1982**, *26*, 483.
[25] J. Krijn, E. J. Baerends, *Fit Functions in the HFS-Method*, Internal Report (in Dutch), Vrije Universiteit Amsterdam, The Netherlands, **1984**.
[26] E. van Lenthe, E. J. Baerends, J. G. Snijders, *J. Chem. Phys.* **1993**, *99*, 4597.
[27] K. Morokuma, *J. Chem. Phys.* **1971**, *55*, 1236.
[28] a) T. Ziegler, A. Rauk, *Inorg. Chem.* **1979**, *18*, 1755; b) T. Ziegler, A. Rauk, *Inorg. Chem.* **1979**, *18*, 1558.
[29] F. M. Bickelhaupt, E. J. Baerends, in *Reviews in Computational Chemistry*, vol. 15, Wiley-VCH, New York, **2000**, pp. 1.
[30] F. M. Bickelhaupt, N. M. M. Nibbering, E. M. Van Wezenbeek, E. J. Baerends, *J. Phys. Chem.* **1992**, *96*, 4864.
[31] G. Te Velde, F. M. Bickelhaupt, E. J. Baerends, C. Fonseca Guerra, S. J. A. Van Gisbergen, J. G. Snijders, T. Ziegler, *J. Comput. Chem.* **2001**, *22*, 931.
[32] a) G. Frenking, K. Wichmann, N. Fröhlich, C. Loschen, M. Lein, J. Frunzke, J. V. M. Rayón, *Coord. Chem. Rev.* **2003**, *238–239*, 55; b) M. Lein, G. Frenking, in *Theory and Applications of Computational Chemistry: The First 40 Years*, p. 367 (Eds.: C. E. Dykstra, G. Frenking, K. S. Kim, G. E. Scuseria), Elsevier, Amsterdam, **2005**.
[33] G. Frenking, K. Wichmann, N. Fröhlich, J. Grobe, W. Golla, D. Le Van, B. Krebs, M. Läge, *Organometallics* **2002**, *21*, 2921.
[34] For a detailed analysis of the EDA terms see: A. Krapp, F. M. Bickelhaupt, G. Frenking, *Chem. Eur. J.* **2006**, *12*, 9196.
[35] G. Frenking, N. Fröhlich, *Chem. Rev.* **2000**, *100*, 717.

Received: December 23, 2008
Published Online: March 12, 2009

